DISSERTATION PROPOSAL (September 15, 2009)

Search for Supersymmetry Using Diphoton Events in $p\bar{p}$ Collisions at $\sqrt{s} = 1.96$ TeV

Eunsin Lee
Department of Physics
Texas A&M University, College Station, TX 77843-4242

We present the results of a search for supersymmetry with gauge-mediated breaking and $\tilde{\chi}_1^0 \to \gamma\tilde{G}$ in the $\gamma\gamma$+missing transverse energy final state. In 2.6±0.2 fb^{-1} of $p\bar{p}$ collisions at $\sqrt{s}$=1.96 TeV recorded by the CDF II detector we observe no candidate events, consistent with a standard model background expectation of 1.4±0.4 events. We set limits on the cross section at the 95% C.L. and place the world's best limit of 149 GeV/c^2 on the $\tilde{\chi}_1^0$ mass at $\tau_{\tilde{\chi}_1^0}$=0 ns. We also exclude regions in the $\tilde{\chi}_1^0$ mass-lifetime plane for $\tau_{\tilde{\chi}_1^0} \lesssim 2$ ns.

INTRODUCTION

The Standard Model (SM) of elementary particles has been enormously successful, but it is incomplete. For theoretical reasons [1], and because of the '$ee\gamma\gamma$+missing transverse energy ($\not\!\!E_T$)' [2] candidate event recorded by the CDF detector in RUN I [3], there is a compelling rationale to search in high energy collisions for the production of heavy new particles that decay producing the signature of $\gamma\gamma + \not\!\!E_T$.

An example of a theory that would produce such events is gauge mediated supersymmetry breaking (GMSB) [1] with $\tilde{\chi}_1^0 \to \gamma\tilde{G}$ where the $\tilde{\chi}_1^0$ is the lightest neutralino and the next-to-lightest supersymmetric particle (NLSP) and the $\tilde{G}$ is a gravitino which is the lightest supersymmetric particle (LSP). These models solve the "naturalness problem" [4] and provide a warm dark matter candidate that is both consistent with inflation and astronomical observations [5]. Since many versions of these models have a similar phenomenology, we consider a scenario in which the lightest neutralino ($\tilde{\chi}_1^0$) decays almost exclusively (>96%) into a photon (γ) and a weakly interacting, stable gravitino ($\tilde{G}$). The $\tilde{G}$ gives rise to $\not\!\!E_T$ by leaving the detector without depositing any energy [6].

In these models, above the current limits from recent experiments [7], the $\tilde{\chi}_1^0$ is restricted to be well above 100 GeV and is favored to have a lifetime on the order of a nanosecond; the $\tilde{G}$ is restricted to have a mass in the range $0.5 < m_{\tilde{G}} < 1.5$ keV/c^2 [8]. At the Tevatron sparticle production is predicted to be primarily into gaugino pairs (see Figure 1), and the $\tilde{\chi}_1^0$ mass ($m_{\tilde{\chi}_1^0}$) and lifetime ($\tau_{\tilde{\chi}_1^0}$) are the two most important parameters in determining the final states and their kinematics [1]. Depending on how many of the two $\tilde{\chi}_1^0$'s decay inside the detector, the event has the signature $\gamma\gamma + \not\!\!E_T$, $\gamma + \not\!\!E_T$ or $\not\!\!E_T$ with one or more additional high E_T particles from the other gaugino pairs. Different search strategies are required for $\tilde{\chi}_1^0$ lifetimes above and below about a nanosecond [12]. Previous searches have been performed for low lifetime models in $\gamma\gamma + \not\!\!E_T$ [9, 10] and nanosecond lifetime models in the delayed $\gamma + jet + \not\!\!E_T$ [7, 11] final state.

In this analysis we focus on the $\gamma\gamma + \not\!\!E_T$ final state, as recommended in [12], for low lifetime, high-mass models of the $\tilde{\chi}_1^0$. The new features of our analysis since the last $\gamma\gamma + \not\!\!E_T$ search with 202 pb^{-1} using the CDF detector [13] are to use the EMTiming system [14] and a new *Met Resolution Model* [15]. We also use 13 times the data (2.6 fb^{-1}). These additions significantly enhance our rejection of backgrounds from instrumental and non-collision sources, which allows us to considerably extend the sensitivity of the search for large $\tilde{\chi}_1^0$ masses compared to previous Tevatron searches [10]. We also extend the search by considering $\tilde{\chi}_1^0$ lifetimes up to 2 ns which are favored for larger $m_{\tilde{\chi}_1^0}$.

There are 6 parameters in the model that determine the masses and lifetimes. For concreteness we use the Snowmass Slope constraint (SPS 8) [6]. This provides additional relationships between the parameters which are typical for the same $\tilde{\chi}_1^0 \to \gamma\tilde{G}$ phenomenology to help focus the search as well as to quote results as a function of $\tilde{\chi}_1^0$ mass and lifetime for the future research. While GMSB provides a useful model we work hard to keep our search as model-independent as possible by keeping our topological requirements to a minimum. In particular we keep a quasi model-independent, signature-based approach in our search, while providing useful benchmarks to compare our sensitivity with our previous searches as well as other searches at DØ [10] and LEP II [7].

Here we briefly describe the aspects of the detector [13] relevant to this analysis. The magnetic spectrometer consists of tracking devices inside a 3-m diameter, 5-m long superconducting solenoid magnet that operates at 1.4 T. A 3.1-m long drift chamber (COT) with 96 layers of sense wires measures the z position, time of the $p\bar{p}$ interaction, and the momenta of charged particles. The calorimeter consists of projective towers with electromagnetic (EM) and hadronic (HAD) compartments and is divided into a central barrel that surrounds the solenoid coil ($|\eta|$<1.1) [2] and a pair of

end-plugs that cover the region $1.1<|\eta|<3.6$. The calorimeters are used to identify and measure the 4-momenta of photons, electrons, and jets (j) [16] and provide $\not\!\!E_T$ information. The EM calorimeter is instrumented with a timing system, EMTiming [14], that measures the arrival time of photons.

Our analysis begins by defining a preselection sample by selecting events with two isolated, central ($|\eta| \lesssim 1.0$) photons with $E_T > 13$ GeV. All candidates are required to pass the standard CDF diphoton triggers, global event selection, standard photon ID, and non-collision background rejection requirements, see Table 1 [9, 15].

The final signal region for this analysis is defined by the subsample of preselection events that also pass a set of optimized final kinematic requirements. The methods for determining the background in the signal region are based on a combination of data and Monte Carlo (MC) simulation and allow for a large variety of potential final sets of kinematic requirements. We perform an *a priori* analysis in the sense that we blind the signal region and select the final event requirements based on the signal and background expectations alone. We optimize our predicted sensitivity using a simulation of our GMSB model. We then calculate, for each GMSB parameter point, the lowest, expected 95% C.L. cross section limit in the no-signal scenario [17] as a function of the following event variables: MetSig, $\Delta\phi(\gamma_1, \gamma_2)$, and H_T. MetSig stands for $\not\!\!E_T$-Significance and a cut on it is essentially a requirement that the MetSig is a measured $\not\!\!E_T$ in the event to be very significant compared to measurement fluctuations; H_T is defined as sum of E_T of all EM objects such as photons, electron (isolated, $E_T > 13$ GeV and $|\eta| < 1.2$, if any), any jets (with $E_T > 15$ GeV and $|\eta| < 2.4$) and $\not\!\!E_T$. The MetSig cut gets rid of most of the QCD background sources of $\gamma\gamma$ events with no intrinsic $\not\!\!E_T$ in which case an measured $\not\!\!E_T$ would be fake. In GMSB production heavy gaugino pair-production dominates and the gauginos decay to light, but high E_T, final state particles via cascade decays, which give lots of H_T in the signal compared to the SM backgrounds. The $\Delta\phi(\gamma_1, \gamma_2)$ cut reduces events with back-to-back photons from electroweak backgrounds with large H_T as $W \to e\nu$ events that pass the other requirements are typically highly boosted.

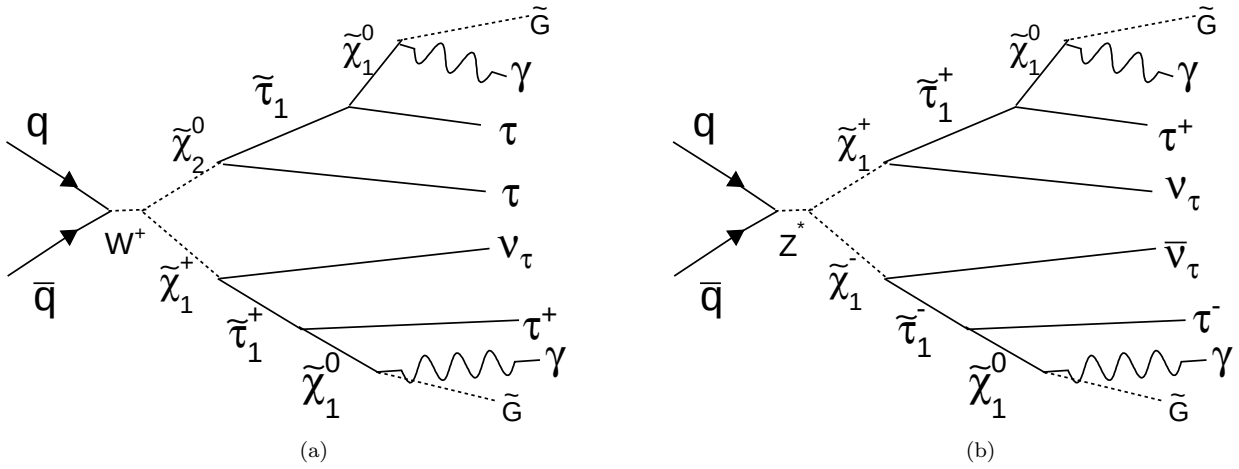

FIG. 1: Feynman diagrams of the dominant tree production processes at the Tevatron for the GMSB model line we consider: $\tilde{\chi}_1^{\pm}\tilde{\chi}_2^0$ (45%) (a) and $\tilde{\chi}_1^{\pm}$ pair (b) production (25%). Note that we only show one choice for the charge.

DATA SELECTION

The analysis is based on 2.59 ± 0.16 fb^{-1} of data delivered to the CDF detector in Run II. The analysis selection begins with events that pass the CDF diphoton triggers which is effectively 100% efficient for the final diphoton selection requirements. We require both highest-E_T photons to be in the fiducial part of the detector with $|\eta| \leq 1.1$, pass the standard photon ID and isolation requirements and have $E_T^{\gamma} > 13$ GeV. In addition to the standard photon ID requirements we have added additional requirements to suppress photomultiplier tube (PMT) high-voltage breakdowns ("spikes") [11] and electron rejection requirements [11] to remove events where an electron fakes a prompt photon (Phoenix tracking rejection). Each event is required to have at least one high quality vertex with $|z_{vx}| \leq 60$ cm. The E_T of all calorimeter objects (individual towers, photons, electrons, and jets) are calculated with respect to the highest $\sum P_T$ vertex. However, an incorrect vertex can be selected when two or more collisions occur in one beam-bunch crossing, making it possible that the highest reconstructed $\sum P_T$ vertex does not produce the photons. If assigning the photons to a different vertex lowers the $\not\!\!E_T$, we take that $\not\!\!E_T$ and the photon E_T's to be from that vertex for all

Requirements	Signal sample (events passed)
Trigger, Goodrun, and Standard photon ID ($\|\eta\|$<1.1, E_T>13 GeV)	45,275
Electron rejection (Phoenix tracking)	41,418
PMT spike rejection	41,412
Vertex requirements	41,402
E_T^{swap}>13 GeV after vertex re-assignment	39,719
Beam Halo rejection	39,713
Cosmic rejection (EMTiming cut)	39,663
$\not\!\!E_T$ cleanup cuts	38,053

TABLE I: Summary of the $\gamma\gamma$ presample selection requirements and the event sample reduction.

calculations (Vertex Re-assignment).

Additional standard selection requirements are placed to reduce non-collision backgrounds, such as cosmic rays and beam-related (beam halo) effects [11]. Photon candidates from cosmic rays are not correlated in time with collisions and events are removed if the timing of either photon, corrected for average path length (t_γ), has $t_\gamma > 4\sigma_t$ or $|t_{\gamma 1} - t_{\gamma 2}| > 4\sigma_{|t_1 - t_2|}$, where $\sigma_t = 1.66$ ns and is a measurement of consistency with being from the collision and $\sigma_{|t_1-t_2|} = 1.02$ ns. Photon candidates can also be produced by beam-related muons that originate upstream of the detector (from the more intense p beam) and travel through the calorimeter, typically depositing small amounts of energy near $\phi \approx 0$ for geometrical reasons. These are suppressed using standard beam halo identification requirements [11]. We also apply $\not\!\!E_T$ quality requirements (cleanup) to remove events if a) there is evidence that the second photon (γ_2) is partially lost in a crack between detector components and has $|\Delta\phi(\not\!\!E_T, \gamma 2)| < 0.3$, or b) the event has a jet, with $E_T^{\rm jet} > 5$ GeV, $|\eta| < 2.5$ is partially lost and has $|\Delta\phi(\not\!\!E_T, jet)| < 0.3$. Our pre-selection sample consists of 38,053 events left after all the quality, ID and cleanup requirements are applied. Table I gives a summary of the event reduction.

BACKGROUNDS

There are three major sources of background for $\gamma\gamma + \not\!\!E_T$ events: QCD events with fake $\not\!\!E_T$, electroweak events with real $\not\!\!E_T$, and non-collision events (PMT spikes, cosmic ray or beam-halo events where one or more of the photons and $\not\!\!E_T$ are not related to the collision).

Standard Model QCD sources, $\gamma\gamma$, $\gamma - jet \rightarrow \gamma\gamma_{fake}$, and $jet - jet \rightarrow \gamma_{fake}\gamma_{fake}$, are the dominant producer of events in the diphoton final state and a major background for $\gamma\gamma$ with fake $\not\!\!E_T$. These backgrounds come in two different categories; fake $\not\!\!E_T$ due to energy measurement fluctuations in the calorimeter and fake $\not\!\!E_T$ due to pathologies such as picking the wrong vertex in events where the true collision did not create a vertex or tri-photon events with a lost photon. The energy measurement fluctuations in the calorimeter, which lead to considerable values of fake $\not\!\!E_T$, are one of the largest backgrounds and are often just due to large fluctuations of large amounts of energy (H_T) deposited in the calorimeter. However, we can significantly reduce the QCD background by selecting events based on MetSig where the amount of $\not\!\!E_T$ is measured to be significantly different from zero according to measurement uncertainties, using a new *Met Resolution Model* [15].

To estimate the background due to energy measurement fluctuations we use the *Met Resolution Model*. The *Met Resolution Model* considers the clustered and unclustered energy in the event and calculates a probability, $P(\not\!\!E_T^{fluct} > \not\!\!E_T)$, for fluctuations in the energy measurement to produce $\not\!\!E_T^{fluct}$ equivalent to or larger than the measured $\not\!\!E_T$. This probability is then used to define MetSig $= -\log_{10}\left(P_{\not\!\!E_T^{fluct} > \not\!\!E_T}\right)$. Events with true and fake $\not\!\!E_T$ of the same value should have, on average, different MetSig. For each data event we throw 10 pseudo-experiments to generate a $\not\!\!E_T$ and calculate its significance, according to the jets and underlying event configuration. Then we count the number of events in the pseudo-experiments that pass our MetSig and other kinematic requirements. This number, divided by the number of pseudo-experiments, gives us the *Met Model* prediction for a sample. The systematic uncertainty on the number of events above a MetSig cut is evaluated by comparing the *Met Model* predictions with the default set of model parameters to predictions obtained with the parameters deviated by $\pm\sigma$. The total uncertainty is estimated by adding the statistical uncertainty on the number of pseudo-experiments passing the cuts and these systematic uncertainties in quadrature.

A source of QCD background that is unaccounted for by the *Met Model* is diphoton candidate events with event

reconstruction pathologies such as a wrong choice of the primary interaction vertex or tri-photon events with a lost photon. To obtain the prediction for the number of events with significant reconstruction pathologies in the QCD background at the same time, we model the kinematics and event reconstruction using a MC simulation of events with in the detector using PYTHIA [18] and a GEANT-based detector simulation [19]. We simulate a sample of SM $\gamma\gamma$ events, with large statistics, and normalize to the number of events in the presample to take into account jet backgrounds which should have similar detector response. Then we subtract off the expectations for energy mismeasurement fluctuations in the MC to avoid double counting. The remaining prediction is due to pathologies alone. The systematic uncertainties on this background prediction include the uncertainty on the scale factor and the uncertainty due to MC-data differences in the unclustered energy parameterization and the jet energy scale.

Electroweak processes involving W's and Z's are the most common source of real and significant $\not\!\!E_T$ in $p\bar{p}$ collisions. We estimate the background rate from decays into both charged and neutral leptons using a combination of data and MC methods. There are four ways we can get a $\gamma\gamma + \not\!\!E_T$ signature in electroweak events that decay into one or more charged leptons: 1) from $W\gamma\gamma$ and $Z\gamma\gamma$ events where both photons are real; 2) from $W\gamma$ and $Z\gamma$ events with a fake photon; 3) from W and Z events where both photon candidates are fake photons; and 4) $t\bar{t}$ production and decay. To estimate the contribution from the electroweak backgrounds we use the Baur [20] and PYTHIA MC's along with a detector simulation, according to their production cross section and k-factors (the ratio of the next-to-leading order (NLO) cross section to the leading order cross section), but normalized to data. The Baur MC simulation of $W\gamma$ and $Z\gamma$ are used to evaluate contributions from both $W/Z+\gamma$ and $W/Z+\gamma\gamma$ events using initial and final state radiations (ISR/FSR). Inclusive W and Z samples produced from PYTHIA are used to obtain the contribution from $W + jet$ and $Z + jet$ events where both photon candidates are fakes, and separately from $t\bar{t}$ production and decay events. To estimate the electroweak backgrounds from neutral leptonic channels such as $Z\gamma\gamma \to \nu\bar{\nu}\gamma\gamma$, $Z\gamma \to \nu\bar{\nu}\gamma + \gamma_{fake}$ or $Z \to \nu\bar{\nu} + \gamma_{fake}\gamma_{fake}$, we use a custom inclusive PYTHIA $Z \to \nu\bar{\nu} + \gamma$ sample. The normalization of the MC results to data is done to take into account MC-data difference and is estimated using the equation:

$$\mathrm{N}^{\mathrm{EWK}}_{\mathrm{signal}} = \sum_{i=0}^{n} \mathrm{N}^{\mathrm{EWK-MC}}_{\mathrm{signal},i} \cdot \mathrm{SF}_i \cdot \left(\frac{\mathrm{N}^{\mathrm{Data}}_{e\gamma,\mathrm{signal}}}{\mathrm{N}^{\mathrm{MC}}_{e\gamma,\mathrm{signal}}} \right) \tag{1}$$

where $\mathrm{N}^{\mathrm{EWK-MC}}_{\mathrm{signal},i}$ is the number of MC events passing all the final kinematic cuts from MC sample i, for each electroweak source. The scale factors, SF_i, normalizes each electroweak background to its production cross section and k-factor. To minimize the dependence of our predictions on potential "MC-data" differences, we normalize, using the rate of the number of $e\gamma$ events observed in the data that also pass all signal kinematic cuts, to the number of events observed in MC. This $e\gamma$ sample is derived from diphoton trigger datasets and the events are required to pass the preselection requirements where electrons are required to pass photon-like ID requirements [15]. The uncertainty on the electroweak backgrounds are dominated by the $e\gamma$ normalization factor uncertainty. This includes data and MC statistical uncertainties as well as differences in MC modeling. The total uncertainties also include the MC statistical uncertainties and uncertainties on the normalization factors added in quadrature.

Non-collision backgrounds coming from cosmic rays and beam-related effects can produce $\gamma\gamma+\not\!\!E_T$ candidates. The dominant source of beam halo events that fake the $\gamma\gamma + \not\!\!E_T$ final state occur when high energy muons, produced in beam-beam pipe interactions, interact with the calorimeter and fake two photons [11]. To estimate the rate at which the B.H. events contribute to the $\gamma\gamma + \not\!\!E_T$ final state, we use a beam halo enriched $\gamma\gamma$ sample selected as having two photon candidates with loose photon ID requirements, but also identified as being due to a beam halo (used to reject beam halo backgrounds). To increase the statistics we do not require a vertex, nor do we reject events that fail the EMTiming requirements. To take this sample to the prediction of the number of events in the signal region we multiply by the measured rate at which these events pass the kinematic requirements as well as the rate they pass the ID and isolation, vertex and timing requirements. Finally we take into account the efficiency for B.H. events to be in this sample. The uncertainties on background rate in the signal region are dominated by the statistical uncertainty on the number of events after all kinematic requirements in the B.H. control sample. The other source of uncertainty, though much smaller, is the uncertainty on the fraction of B.H. events that pass the vertex, ID and EMTiming requirements.

The dominant source of cosmic ray muon events that fake the $\gamma\gamma + \not\!\!E_T$ signature come via photon Bremsstrahlung as the muon traverses the magnet, or by catastrophic interaction with the EM calorimeter. To estimate the rate which these backgrounds enter the signal region we select a cosmic ray enriched sample of two photons passing the loose photon ID requirements, but failing the timing requirements. Specifically, at least one of the photon candidate must have $\mathrm{T}_\gamma > 25$ ns. That way we take into account all cosmic ray sources; both photons from the same cosmic ray, both photons from different cosmic rays, and one photon from a cosmic ray and one from the collision or the pair must have $|\Delta \mathrm{T}_{\gamma\gamma}| > 8$ ns. To increase the sample statistics, events are not required to pass our vertex requirement

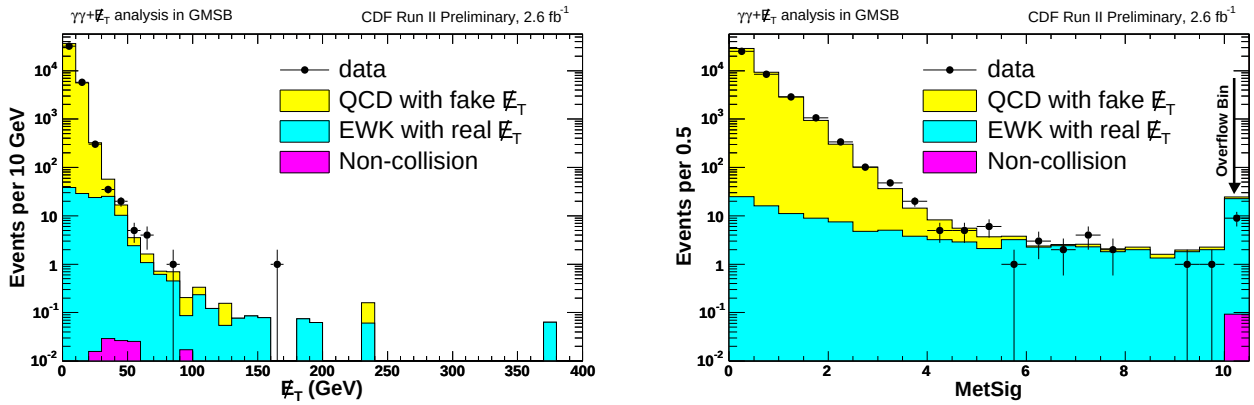

(a) (b)

FIG. 2: The background predictions of (a) $\not\!\!E_T$ and (b) MetSig for the presample. The highest MetSig bin includes all overflow events.

($|Z_{vx}| < 60$ cm), which we correct for in our sample estimate, using similar techniques as for beam halo. The uncertainties are dominated by the statistical uncertainty on the number of identified cosmic ray events.

After estimating the MetSig distributions for all the backgrounds, where the QCD is normalized to the data in the low MetSig region where the EWK backgrounds are expected to be negligible, the expected MetSig distribution for the presample is shown in Figure 2, also showing $\not\!\!E_T$. With these tools in hand we are set to estimate the backgrounds for a large variety of kinematic requirements and move to an estimation of the acceptance for GMSB models in the signal region for use in optimization.

GMSB SIGNAL MONTE CARLO AND SYSTEMATIC UNCERTAINTIES

To estimate the acceptance for GMSB we use the PYTHIA event generator as well as a full detector simulation. The acceptance, used in the optimization procedure and limit setting, is taken to be equal to the ratio of simulated events that pass all the requirements to all events produced. The fraction of $\tilde{\chi}_1^0$ decays that occur in the detector volume, and thus the acceptance, are dependent on both the lifetime and the masses of the sparticles [12]. For the purpose of this analysis we consider a GMSB model with parameters fixed on the minimal-GMSB Snowmass slope constraint (SPS 8) that is commonly used [7, 9] and take the messenger mass scale $M_{\rm m}$=2Λ, tan(β)=15, μ>0 and the number of messenger fields $N_{\rm m}$=1. The $\tilde{G}$ mass factor and the supersymmetry breaking scale Λ are allowed to vary independently. All SUSY production processes are simulated to maximize our sensitivity to the model [21]. The breakdown of events after passing each of the selection requirements for an example GMSB point at $m(\tilde{\chi}_1^0) = 140$ GeV and $\tau(\tilde{\chi}_1^0) = 0$ ns near the limit, is shown in Table II. For completeness we have included the results for the final event selection, determined in next Section.

Requirement	**Events passed**	$A_{\rm Signal\ MC}$**(%)** ($m(\tilde{\chi}_1^0)$=140 GeV and $\tau(\tilde{\chi}_1^0)$=0 ns)
Sample events	133330	100.0
Two EM Objects and $\lvert z_{vertex}\rvert < 60$ *cm*	124771	93.6
Photon fiducial and Standard ID cuts ($\lvert\eta\rvert < 1.1$ and $E_T > 13$ GeV)	18270	13.7
Phoenix Rejection & PMT cuts	17625	13.2
Beam Halo and Cosmic Rejection cuts	17612	13.2
Vertex Swap and $\not\!\!E_T$ Cleanup cuts	17049	12.8
MetSig>3	12610	9.5
H_T>200 GeV	11913	8.9
$\Delta\phi(\gamma_1,\gamma_2)<\pi-0.35$	10395	7.8

TABLE II: Summary of the event reduction for a GMSB example point in the $\gamma\gamma$+$\not\!\!E_T$ final state. We have included the final, optimized cuts for completeness.

Since we estimate the sensitivity of the search to be equal to the expected 95% C.L. cross section limits with the no signal hypothesis, we need the uncertainties for the trigger, luminosity, background and acceptance. As mentioned in previous Section, with our combination of triggers we take a trigger efficiency of 100% with negligible error [15]. The systematic uncertainty on the luminosity is taken to be 6% with major contributions from the uncertainties on the CLC acceptance from the precision of the detector simulation [19] and the event generator [18]. The systematic uncertainty on the background in the signal region is determined from our understanding of both the collision and non-collision sources as described in previous Section. The background uncertainty is evaluated for every set of cuts in the optimization procedure. The systematic uncertainty on the signal acceptance for an example GMSB point of $m(\tilde{\chi}_1^0) = 140$ GeV and $\tau(\tilde{\chi}_1^0) = 0$ ns is estimated to be 6.9% with major contributions from diphoton ID and isolation efficiency (5.4%) and ISR/FSR (3.9%). The uncertainty on the NLO production cross section is dominated by the uncertainty from parton distribution functions (7.6%) and the renormalization scale (2.6%) for a total of 8.0%. All uncertainties are included in the final cross section limit calculation, and we take the acceptance and production cross section uncertainties in quadrature for a total uncertainty of 10.6%.

OPTIMIZATION AND RESULTS

Now that the background is estimated and the signal acceptance is available for a variety of selection requirements, an optimization procedure can be readily employed to find the optimal selection requirements before unblinding the signal region. We optimize for the following kinematic requirements: MetSig, H_T, and $\Delta\phi(\gamma_1, \gamma_2)$.

As described in earlier section, the MetSig cut gets rid of most of the QCD background with fake $\not\!\!E_T$. The H_T cut separates between the high E_T, light final state particles produced by GMSB events via cascade decays and SM backgrounds, dominated by QCD and electroweak backgrounds, which do not have lots of high E_T objects. The $\Delta\phi(\gamma_1, \gamma_2)$ cut gets rid of events where two photons are back to back since electroweak backgrounds with large H_T are typically a high E_T photon recoiling against $W \to e\nu$, which means the gauge boson decay is highly boosted. Also the high E_T diphoton with large H_T from QCD background are mostly back-to-back with fake $\not\!\!E_T$ or wrong vertex.

By estimating our sensitivity using the 95% C.L. expected cross section limits on GMSB models in the no-signal assumption, we find the optimal set of cuts before unblinding the signal region. We use the standard CDF cross section limit calculator [22] to calculate the limits, taking into account the predicted number of background events, the acceptance, the luminosity and their systematic uncertainties. We take

$$\sigma_{95}^{\exp} = \sum_{N_{obs}=0}^{\infty} \sigma_{95}^{obs}(\text{cut}) \times \text{Prob}(N_{obs}, N_{exp} = \mu)$$

$$\text{RMS}^2 = \sum_{N_{obs}=0}^{\infty} (\sigma_{95}^{obs}(\text{cut}) - \sigma_{95}^{\exp})^2 \times \text{Prob}(N_{obs}, N_{exp} = \mu)$$

where N_{obs} is the number of observed events in the pseudoexperiment, μ is the mean of the number of expected events as a function of the cuts and σ_{95}^{obs} denotes the cross section limit if N_{obs} were observed.

For each GMSB point the minimum expected cross section limit defines our set of optimal requirements for the mass and lifetime combination. The exclusion region is defined by the region where the production cross section is above the 95% C.L. cross section limit. The mass/lifetime limit is where the two cross. Figures 3-(a), (c), and (e) show the expected cross section limit as a function of a kinematic selection requirement after keeping all other requirements fixed at the already optimized values, showing it is at the minimum for a mass-lifetime combination of $m(\tilde{\chi}_1^0) = 140$ GeV and $\tau(\tilde{\chi}_1^0) = 0$ ns, which is near the exclusion region limit.

We decided to use a single set of optimal requirements before we open the box based on the observation that they will yield the largest expected exclusion region. We chose: MetSig>3, H_T>200 GeV, $\Delta\phi(\gamma_1, \gamma_2)<\pi - 0.35$ rad. With these requirements we predict a total of 1.38±0.44 background events. The dominant electroweak contributions are $Z\gamma \to \nu\nu\gamma$ and $Z\gamma \to \mu\mu\gamma$ which produce a total of 0.26±0.08 and 0.19±0.10 events respectively. The QCD background is dominated by energy measurement fluctuations in the $\not\!\!E_T$, estimated using the *Met Model*, to have a rate of 0.46±0.24 events. The non-collision backgrounds are dominated by cosmic ray which have a rate of $0.001^{+0.008}_{-0.001}$ events. Table III provides a summary.

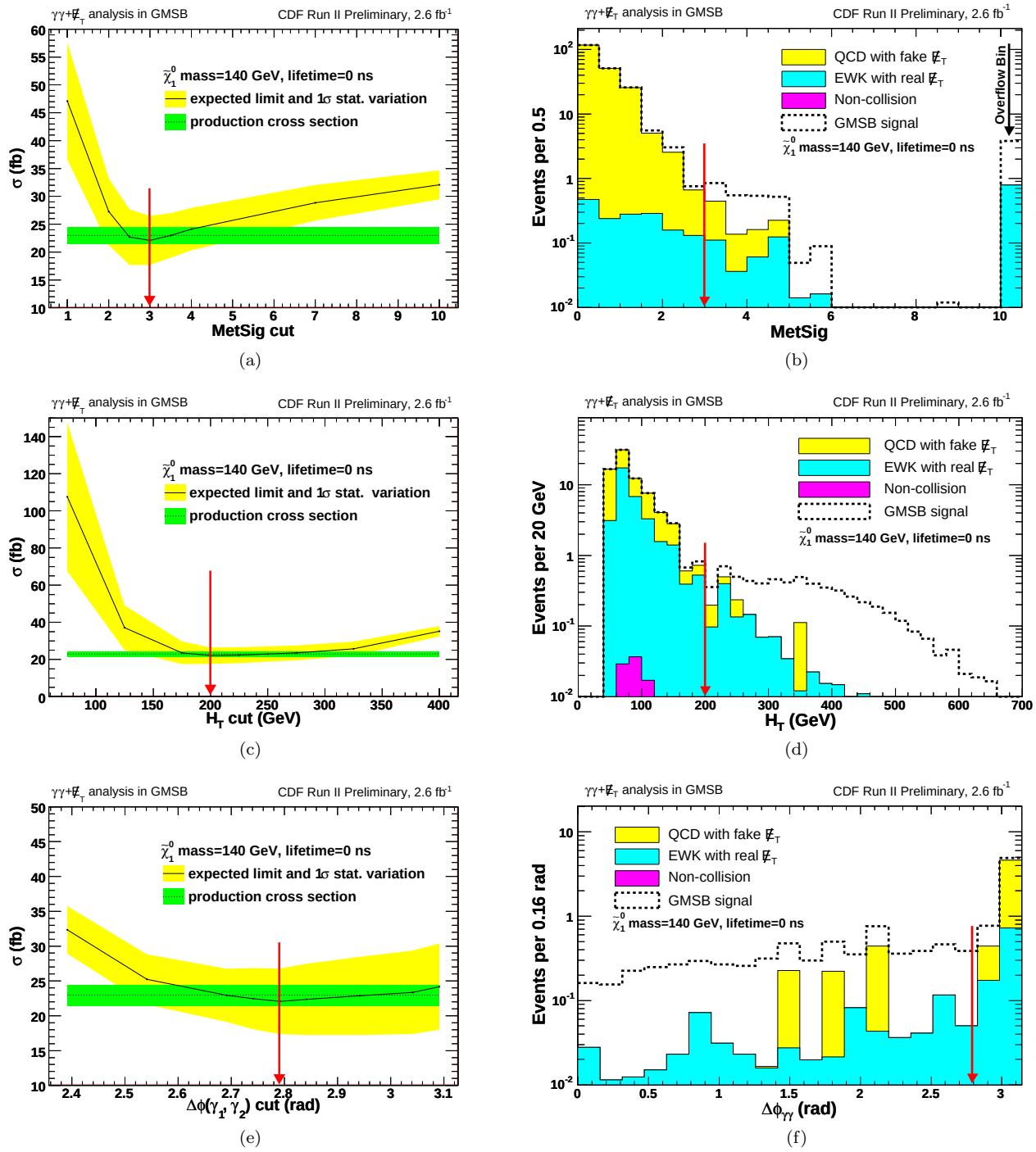

FIG. 3: The expected 95% C.L. cross section limit as a function of the MetSig (a), H_T (c), and $\Delta\phi(\gamma_1, \gamma_2)$ (e) requirements for a GMSB example point ($m(\tilde{\chi}_1^0) = 140$ GeV and $\tau(\tilde{\chi}_1^0) = 0$ ns). All other cuts held at their optimized values. The optimal cut is where the expected cross section is minimized. Indicated in green is the 8.0% uncertainty-band for the production cross section and in yellow is the RMS. The N-1 predicted kinematic distributions after the optimized requirements are shown in Figure (b), (d), and (f). Note that in (b) bins at MetSig=10 are overflows.

Background Source	Expected Rate±Stat±Sys
Electroweak	0.92±0.21±0.30
QCD	0.46±0.22±0.10
Non-Collision	$0.001^{+0.008}_{-0.001} \pm 0.001$
Total	1.38±0.30±0.32

TABLE III: Summary of the combined background estimations after optimization. Note we have ignored the small asymmetric uncertainty in the total calculation.

Figures 3-(b), (d), and (f) show the distributions of each optimization variable normalized to the number of expected events, after applying all optimized cuts. We compare the background distribution before unblinding the signal region and the expected signal in the signal region for an example GMSB point at $m(\tilde{\chi}_1^0) = 140$ GeV and $\tau(\tilde{\chi}_1^0) = 0$ ns. Taking into account the errors we expect an acceptance of (7.8±0.5)% and 4.6±0.6 events for this point.

After all optimal cuts we open the box and observe no events, consistent with the expectation of 1.2±0.4 events. We show the kinematic distributions for the background and signal expectations along with the data in Figure 4. There is no distribution that hints at an excess and the data appears to be well modeled by the background prediction alone.

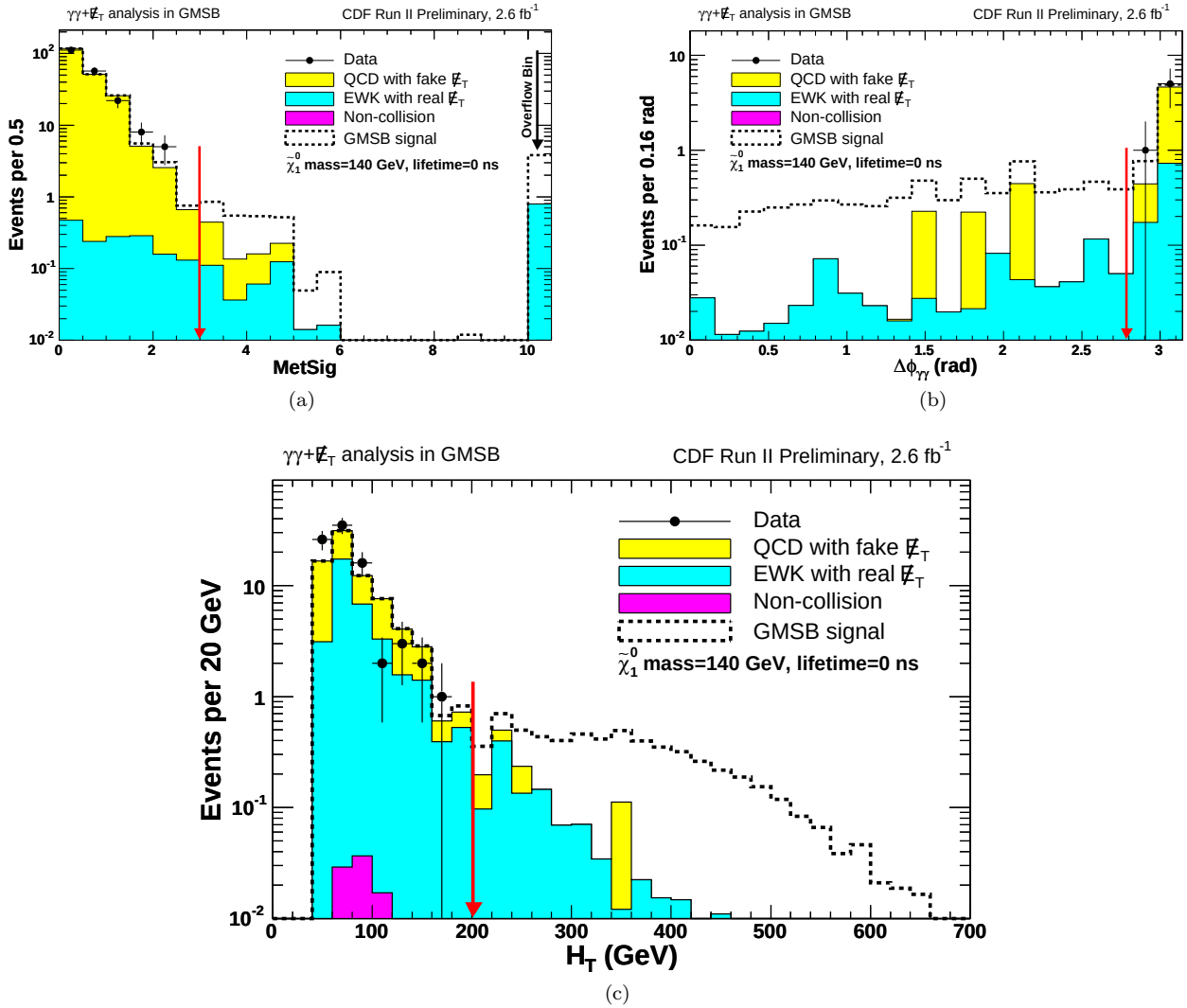

FIG. 4: The same N-1 plots as Figure 3, but including the data. Each variable is plotted through the whole region while holding other variables at the optimal cuts. There is no evidence for new physics and the data is well modeled by backgrounds alone. The highest bin in (a) includes all overflow events.

We show the predicted and observed cross section limits along with the NLO production cross section, which is calculated by multiplying the PYTHIA LO cross section calculation by k-factor [23] in Figure 5. Since the number of observed events is below expectations the observed limits are slightly better than the expected limits. The $\tilde{\chi}_1^0$ mass reach, based on the predicted (observed) number of events is 141 GeV/c^2 (149 GeV/c^2), at a lifetime of 0 and 1 ns. We do not consider lifetimes above 2 ns as the photon ID variables have been shown to not work there and the expectation that most of the parameter space in high lifetimes there should be covered by searches in single delayed photon analysis [11, 12]. We show the 95% C.L. NLO exclusion region as a function of mass and lifetime of $\tilde{\chi}_1^0$ using the fixed choice of cuts from the optimization for both for the predicted and observed number of background events in Figure 6-(a). These limits extend the reach beyond the CDF delayed photon results [11] and well beyond those of DØ searches at $\tau_{\tilde{\chi}_1^0} = 0$ [10] and the limit from ALEPH/LEP [7], and are currently the world's best.

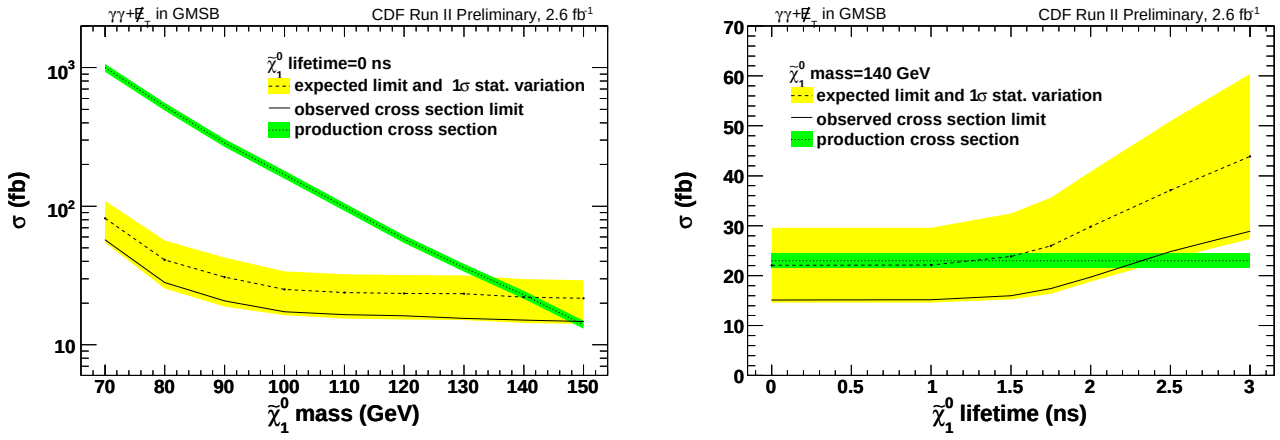

(a) (b)

FIG. 5: The predicted and observed cross section limits as a function of the $\tilde{\chi}_1^0$ mass at a lifetime of 0 ns (a) and as a function of the $\tilde{\chi}_1^0$ lifetime at a mass of 140 GeV/c^2 (b). Indicated in green is the 8.0% uncertainty-band for the production cross section, in yellow the RMS variation in the expected on the cross section limit.

CONCLUSIONS AND PROSPECTS FOR THE FUTURE

We have set limits on GMSB models using the $\gamma\gamma + \not\!\!E_T$ final state. Candidate events were selected based on 13 times more data, the new $\not\!\!E_T$ resolution model technique, the EMTiming system and a full optimization procedure. We found 0 events using 2.6 fb^{-1} of data in run II which is consistent with the background estimate of 1.2±0.4 events from the Standard Model expectations. We showed exclusion regions and set limits on GMSB models with a $\tilde{\chi}_1^0$ mass reach of 149 GeV/c^2 at a $\tilde{\chi}_1^0$ lifetime of 0 ns. Our results extend the world sensitivity to these models.

To investigate the prospects of a search at higher luminosity we calculate the cross section limits assuming all backgrounds scale linearly with luminosity while their uncertainty fractions remain constant. By the end of Run II, with an integrated luminosity of 10 fb^{-1}, we estimate a mass reach of $\simeq$ 160 GeV/c^2 at a lifetime of 0 ns, as shown in Figure 6-(b). For higher lifetimes (above ∼2 ns) the next generation delayed photon analysis will extend the sensitivity taken from Ref. [11] and then will combine these results for completeness.

[1] S. Dimopoulos, S. Thomas, and J. Wells, Nucl. Phys. B **488**, 39 (1997); S. Ambrosanio, G. Kribs, and S. Martin, Phys. Rev. D **56**, 1761 (1997); G. Giudice and R. Rattazzi, Phys. Rep. **322**, 419 (1999); S. Ambrosanio, G. Kane, G. Kribs, S. Martin, and S. Mrenna, Phys. Rev. D **55**, 1372 (1997).

[2] We use a cylindrical coordinate system in which the proton beam travels along the z-axis, θ is the polar angle, ϕ is the azimuthal angle relative to the horizontal plane, and $\eta = -\ln\tan(\theta/2)$. The transverse energy and momentum are defined as $E_T = E\sin\theta$ and $p_T = p\sin\theta$ where E is the energy measured by the calorimeter and p the momentum measured in the tracking system. $\not\!\!E_T = |-\sum_i E_T^i \vec{n}_i|$ where $\vec{n}_i$ is a unit vector that points from the interaction vertex to the i^{th} calorimeter tower in the transverse plane.

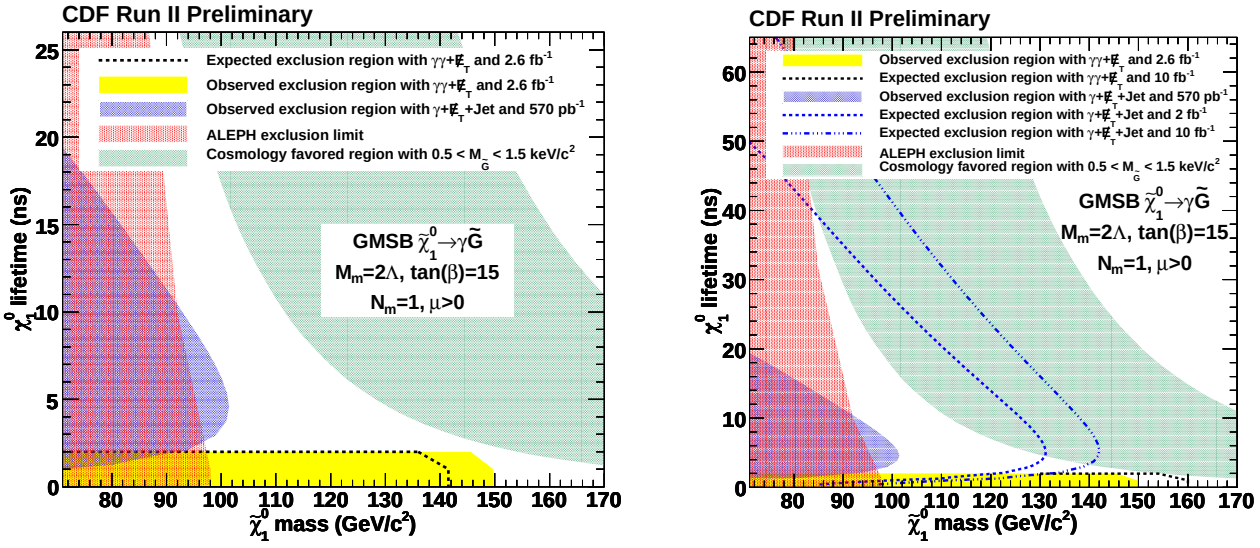

(a) (b)

FIG. 6: The predicted and observed exclusion region along with the limit from ALEPH/LEP [7] and the $\gamma + \not\!\!E_T + jet$ delayed photon analysis [11]. We have a mass reach of 141 GeV/c^2 (predicted) and 149 GeV/c^2 (observed) at the lifetime up to 1 ns. The green shaded band shows the parameter space where $0.5 < m_{\tilde{G}} < 1.5$ keV/c^2, favored in cosmologically consistent models [8] (a). The projected sensitivity to GMSB models with more data. The black dashed line shows the prediction of the exclusion region limit after a scaling of the background prediction and the uncertainties for a luminosity of 10 fb^{-1}. The blue dashed lines show the prediction of the exclusion region limits from the delayed photon analysis for a luminosity of 2 fb^{-1} and 10 fb^{-1} respectively taken from Ref. [11]. (b)

[3] CDF Collaboration, F. Abe *et al.*, Phys. Rev. Lett. **81**, 1791 (1998); Phys. Rev. D **59**, 092002 (1999).
[4] S. Martin, arXiv:hep-ph/9709356.
[5] P. Bode, J. Ostriker, and N. Turok, Astrophys. J. **556**, 93 (2001).
[6] B. C. Allanach *et. al.*, Eur. Phys. J. C**25**, 113 (2002).
[7] ALEPH Collaboration, A. Heister *et. al.*, Eur. Phys. J. C **25**, 339 (2002); A. Garcia-Bellido, Ph.D. thesis, Royal Holloway University of London (2002) (unpublished), arXiv:hep-ex/0212024.
[8] C.-H. Chen and J. F. Gunion, Phys. Rev. D **58**, 075005 (1998).
[9] CDF Collaboration, D. Acosta *et. al.*, Phys. Rev. D **71**, 031104 (2005).
[10] DØ Collaboration, V.M. Abazov *et. al.*, Phys. Lett. B **659**, 856 (2008).
[11] CDF Collaboration, A. Abdulencia *et. al.*, Phys. Rev. Lett **99**, 121801 (2007); CDF Collaboration, T.Aaltonen *et. al.*, Phys. Rev. D **78**, 032015 (2008).
[12] P. Wagner and D. Toback, Phys. Rev. D **70**, 114032 (2004).
[13] D. Acosta *et al.* (CDF Collaboration), Phys. Rev. D **71**, 032001 (2005).
[14] M. Goncharov *et. al.*, NIM A**565**, 543 (2006).
[15] T. Aaltonen *et al.* (CDF Collaboration), *Search for Anomalous Production of Events with Two Photons and Additional Energetic Objects at CDF*, to be submitted to Phys. Rev. D.
[16] For a discussion of the jet energy measurements, see T. Affolder *et al.*(CDF Collaboration), Phys. Rev. D. **64**, 032001 (2001). For a discussion of standard jet correction systematics, see A. Bhatti *et al.*, Nucl. Instrum. Methods, A 566, 375 (2006). We use jets with cone size ΔR=0.4.
[17] E. Boos, A. Vologdin, D. Toback and J. Gaspard, Phys. Rev. D **66**, 013011 (2002).
[18] T. Sjöstrand *et al.*, Comput. Phys. Commun. **135**, 238 (2001). We use version 6.216.
[19] We use the standard GEANT based detector simulation [R. Brun *et al.*, CERN-DD/EE/84-1 (1987)] and add a parametrized EMTiming simulation.
[20] U. Baur, T. Han and J. Ohnemus, Phys. Rev. D **48**, 5140 (1993); U. Baur, T. Han and J. Ohnemus, *ibid.* **57**, 2823 (1998); The $W\gamma$ and $Z\gamma$ processes are simulated using the leading-order event generator and have a k-factor fixed at 1.36. Initial and final state radiation (resulting in additional jets or photons), underlying event, and additional interactions are simulated using PYTHIA [18].
[21] P. Simeon and D. Toback, J. Undergrad. Research in Phys. 20, 1 (2007).
[22] T. Junk, Nucl. Instrum. Methods A**434**, 435-443 (1999).
[23] W. Beenakker, *et al.*, Phys. Rev. Lett. **83**, 3780 (1999).